Electron paramagnetic resonance and theoretical studies of shallow phosphorous centers in 3*C*-, 4*H*-, and 6*H*-SiC

N. T. Son and A. Henry
Department of Physics, Chemistry and Biology, Linköping University, SE-581 83 Linköping, Sweden

J. Isoya, M. Katagiri, and T. Umeda
Research Center for Knowledge Communities, Graduate School of Library, Information and Media Studies, University of Tsukuba, Tsukuba 305-8550, Japan

A. Gali
Department of Atomic Physics, Budapest University of Technology and Economics, Budafoki út 8, H-1111, Budapest, Hungary

E. Janzén
Department of Physics, Chemistry and Biology, Linköping University, SE-581 83 Linköping, Sweden
(Received 22 July 2005; published 1 February 2006)

Continuous-wave (cw) electron paramagnetic resonance (EPR) at both *X*-band and *W*-band frequencies, pulsed-EPR, and pulsed electron nuclear double resonance (ENDOR) were used to study phosphorus shallow donors in 3*C*-, 4*H*-, and 6*H*-SiC doped with phosphorus (P) during chemical vapor deposition (CVD) growth. In 3*C*-SiC, a spectrum with D_{2d} symmetry and the principal g values, $g_{\parallel}=2.0051$, $g_{\perp}=2.0046$, was detected. The ^{31}P hyperfine (hf) constants of the center, $A_{\parallel}=0.53$ MHz and $A_{\perp}=-0.13$ MHz, were determined from pulsed-ENDOR measurements. A doublet with C_{3v} symmetry ($g_{\parallel}=2.0065$, $g_{\perp}=2.0006$, and ^{31}P hf constants $A_{\parallel}=8.24$ MHz, $A_{\perp}=5.89$ MHz) was detected in P-doped 4*H*-SiC. In the 6*H* polytype, the same P_1 and P_2 doublets [Greulich-Weber, Phys. Status Solidi A **162**, 95 (1997)] or dP_h, dP_{c1}, and dP_{c2} doublets [Baranov *et al.*, Phys. Rev. B **66**, 165206 (2002)] previously reported in material doped with P by neutron transmutation were detected. Our cw-EPR, two-dimensional EPR, and electron spin-echo envelope modulation (ESEEM) results confirm that the dP_{c1} and dP_{c2} doublets are related to different allowed and forbidden transitions of the P_2 center with $S=1/2$ and $I=1/2$. Based on the observed ^{31}P hf interaction (for three polytypes) and the ^{13}C hf interaction with nearest neighbors (for 4*H*- and 6*H*-SiC), the P-related spectra are assigned to the ground states of the isolated shallow P at Si site. The valley-orbit splitting of the shallow P donors was estimated from the temperature dependence of the spin-lattice relaxation time and of the cw-EPR signal intensities. Based on the *ab initio* supercell calculations of the spin localizations on the P atom and the nearest C neighbors in 4*H*-SiC and the similarity between the spectra in the 4*H* and 6*H* polytypes, we reassign the spectrum in 4*H*-SiC to the shallow P donor at the quasicubic site (P_k) and the two doublets P_1 and P_2 in 6*H*-SiC to the shallow P donors at two quasicubic sites, P_{k1} and P_{k2}, respectively.

DOI: 10.1103/PhysRevB.73.075201 PACS number(s): 76.30.−v, 71.55.Ht, 71.15.Mb, 61.72.Bb

I. INTRODUCTION

Controlling the conductivity via doping of shallow donors or acceptors is essential for the fabrication of semiconductor devices. In silicon carbide (SiC), nitrogen (N) shallow donors, which substitute for carbon, are easily and unintentionally incorporated during the crystal growth. Phosphorous (P), which is expected to substitute for silicon, is an alternative shallow donor to N in SiC. Due to its higher level of electrical activation, P has advantages over N in the high doping range ($>3\times10^{19}$ cm^{-3}), where the electrical conductivity in N-doped SiC is being saturated.[1]

SiC has many polytypes differing in the stacking sequences of Si-C bilayers. In the cubic lattice of 3*C*-SiC, each silicon and carbon has one site. However, in the hexagonal lattice of 4*H*-SiC, each silicon and carbon has two inequivalent lattice sites called hexagonal (h) and quasicubic (k) sites, which differ from each other by their surrounding arrangement beyond the second neighbors. In the 6*H* polytype, there are one hexagonal (h) and two quasi-cubic (k_1,k_2) sites. A shallow donor occupying different inequivalent lattice sites can have different electronic structure as shown in the case of the shallow N donors, which can be studied by magnetic resonance techniques such as electron paramagnetic resonance (EPR) and electron nuclear double resonance (ENDOR) (see Ref. 2 for a review).

EPR studies of P in SiC have mainly been performed in 6*H*-SiC doped with P by neutron transmutation of ^{30}Si in the host crystal to ^{31}P (Refs. 2–6) or by P ion implantation.[7,8] These doping techniques and the required high-temperature annealing are known to introduce also intrinsic defects and their associated complexes. The detection of P involving in a paramagnetic center is based on the observation of ^{31}P ($I=1/2$, natural abundance 100%) hyperfine (hf) interaction. Unfortunately, in these studies, the identification of the substitutional site of P was severely hampered by the interference of strong EPR signals of N donors in the host crystal and by the complexity of the presence of additional deep

 ©2006 The American Physical Society

defect centers such as residual lattice damages and their associated complexes. Until the recent theoretical study,[9] which pointed out that a considerable fraction of P might end up in occupying the carbon site after high-temperature annealing required in these doping methods, P involved in the observed P-related EPR centers in neutron-transmuted 6*H*-SiC had always been assumed to substitute for silicon. The labeling and interpretation of reported EPR spectra are controversial. In the first EPR study of neutron-transmuted 6H-SiC,[3] the P_1 ($A_\parallel$=5.63 mT, $A_\perp$=5.55 mT), and P_2 ($A_\parallel$=5.17 mT, $A_\perp$=5.17 mT) spectra observed at 77 K were suggested to be related to the shallow P donors occupying the k_1, k_2, and the h sites, respectively, and the P+V spectrum ($A_\parallel$=0.92 mT, $A_\perp$=0.72 mT) was assigned to a complex involving P and a vacancy. The P_1, P_2 centers were later labeled P_a and P_b and were attributed to the excited state of the shallow P donors, whereas two other spectra [originally labeled I_1 and I_2 (Ref. 4) and later changed to P_1 and P_2 (Refs. 2 and 5)] observed at low temperatures ($T<10$ K) were assigned to the ground state of the shallow P donors with P_1 corresponding to P on the h site and P_2 to P on the k_1, k_2 sites of the Si sublattice.[2,5] In a later EPR study,[6] both sets of low- and high-temperature P-related centers were simultaneously observed at 4.2 K, excluding the possibility that the P_a and P_b are related to the excited states as proposed in Ref. 2. The P_a, P_b and P+V centers were instead reassigned to the ground state of the shallow P donors at the cubic and hexagonal sites of Si sublattice and labeled sP_{c1}, sP_{c2}, and sP_h.[6] Also in these *X*-band EPR experiments,[6] the P_2 doublet[2,5] was suggested to be contributed from two overlapping spectra, labeled dP_{c1} and dP_{c2}. Based on the observation of their satellites, which were attributed to the hf interaction with one ^{29}Si nucleus, the low-temperature spectra, P_1 and P_2 (or I_1 and I_2), in Refs. 2 and 5 were assigned to deep level complex defects involving P at the Si site (P_{Si}) and the carbon vacancy (V_C), (P_{Si}-V_C), at three inequivalent silicon sites in 6*H*-SiC with new labels dP_h ($A_\parallel$=0.10 mT, $A_\perp$=0.05 mT), dP_{c1} ($A_\parallel$=0.62 mT, $A_\perp$=0.38 mT), and dP_{c2} ($A_\parallel$=0.48 mT, $A_\perp$=0.19 mT).[6] Recent EPR studies on P-ion implanted 6*H*-SiC (Refs. 7 and 8) also used the assignment that the P_a and P_b centers were the ground state of the shallow P donors at Si site and estimated their valley-orbit splitting. The sum of the concentrations of P_a and P_b corresponded to only ~0.08 of the implanted P ions in the samples annealed at 1650 °C after the implantation at 800 °C. Optically detected EPR of 6*H*-SiC doped with P during sublimation growth[10] was reported but the nature of these broad signals is still unclear. In sublimation-grown samples, the concentration of the shallow N donors was often rather high (similar or orders of magnitude higher than that of the shallow P donors), giving rise to the strong EPR signals of the shallow N donors. The P-related EPR signals were therefore obscured by strong N spectra and could hardly be studied.[11] In recent calculations,[9] the P-related centers with small (P_1, P_2) and large (P_a, P_b) hf constants were reassigned to the shallow P donors occupying Si and C lattice sites, respectively. In *in situ* P-doped sublimation-grown 6*H*-SiC, only the strong EPR signals of the N donors and two weak shoulders, which were believed to be the fingerprint of the P+V center, were detected. Therefore it was suggested that the amount of electrically active isolated P incorporated during growth is insignificant and P may form diamagnetic complexes.[9]

In our preliminary studies,[12] we observed the EPR spectra P_1 and P_2 (Refs. 2 and 5) or dP_h, dP_{c1}, and dP_{c2} (Ref. 6) in 6*H*-SiC doped with P during chemical vapor deposition (CVD) growth.[13] We followed the site assignment of Ref. 2 that the P_2 (or dP_{c1} and dP_{c2}) doublet corresponds to the P substituting for Si at the k_1 and k_2 sites, and the strong angular dependence of the signal intensity of the dP_{c1} and dP_{c2} doublets remains unexplained.

In this paper, we study 3*C*-, 4*H*-, and 6*H*-SiC doped with P during CVD growth using continuous-wave (cw) EPR, electron spin-echo (ESE) detected EPR, electron spin-echo envelope modulation (ESEEM), two-dimensional (2D) EPR, and pulsed ENDOR. In our pure CVD freestanding layers, the P spectra can be observed without interference from other EPR signals such as the shallow N donors in the sublimation-grown material or N and radiation induced defects in neutron transmuted and P-implanted materials. Therefore we could detect clear hf structure due to the interaction with nearest-neighbor C atoms in 4*H*- and 6*H*-SiC and unambiguously identify the shallow P donors occupying the Si sublattice. Section III presents experimental results in 6*H*-SiC confirming that (i) the P_1 and P_2 centers[2,5] (i.e., I_1 and I_2 centers[4] or dP_h, dP_{c1}, and dP_{c2} centers in Ref. 6) are related to the ground state of P occupying the Si sublattice, (ii) the P_2(Ref. 2) (or dP_{c1} and dP_{c2} (Ref. 6)) doublet is not arising from two different P centers but correspond to allowed and forbidden transitions of one P center with $S=1/2$ and $I=1/2$. In this section, EPR and ENDOR results of P in 3*C*- and 4*H*-SiC were presented. We also show that the P centers in 3*C*-, 4*H*-, and 6*H*-SiC exhibit features characteristic of having a low-lying excited state. The energy separation between the ground state and the excited state has been estimated from the temperature dependence of the EPR signal intensity and of the spin-lattice relaxation time. In Sec. IV, the theoretical studies of the spin localizations on the P atoms and the nearest-neighbor C atoms of the shallow P donors in 4*H*-SiC are presented. The assignment of P centers to the shallow P donors occupying different inequivalent lattice sites and their electronic structure are discussed in Sec. V.

II. EXPERIMENT

In order to avoid the interference from N and other defects, which can be introduced during neutron transmutation or P ion implantation and subsequent high-temperature annealing, we used high-purity 3*C*-, 4*H*- and 6*H*-SiC layers doped with P during CVD growth.[13] In 4*H*- and 6*H*-SiC layers, the concentration of shallow P donors was about $1-4\times10^{16}$ cm^{-3} as determined from secondary ion-mass spectrometry (SIMS),[13] and from capacitance versus voltage (CV) measurements. In 3*C*-SiC epitaxial layers, the P concentration is estimated to be in the 10^{17}-cm^{-3} range. The concentration of the shallow N donors is in the low 10^{14}-cm^{-3} range for 4*H*- and 6*H*-SiC. The N-doped *n*-type substrate was removed by polishing in order to eliminate the

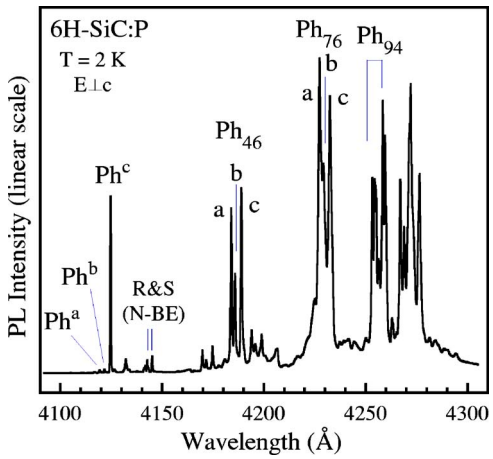

FIG. 1. (Color online) PL spectrum of P bound excitons in a 6*H*-SiC CVD layer measured with polarization $\mathbf{E}\perp\mathrm{c}$ at 2 K, showing no-phonon lines (Ph^a, Ph^b, and Ph^c) and their phonon replicas. The subscript number denotes the phonon energy in meV. Weak no-phonon lines *R* and *S* of the N-bound excitons (NBE) are indicated.

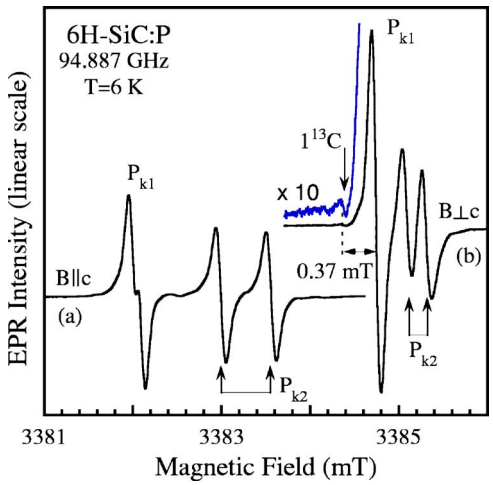

FIG. 2. (Color online) High-frequency EPR spectra in P-doped 6*H*-SiC freestanding layers measured at 6 K for (a) $\mathbf{B}\|\mathbf{c}$ and (b) $\mathbf{B}\perp\mathbf{c}$. The ^{13}C hf line due to one nearest-neighbor C atom of the P_{k1} center can be seen in the $\times 10$ scale.

interference from the EPR spectra of the N donors. The thickness of the freestanding layers was about 150 μm.

The cw-EPR measurements were performed on a Bruker ELEXSYS E580 *X*-band (~9.75 GHz) spectrometer and on a home-built *W*-band (~95 GHz) setup. The pulsed experiments such as echo-detected EPR, inversion-recovery, ESEEM, pulsed-ENDOR, and two-dimensional (2D) EPR were also performed on the ELEXSYS E580 spectrometer. In the pulsed experiments, we used the microwave pulse with the magnetic field $B_1\sim 0.5$ mT. The echo intensity was obtained by integrating the echo signal within the range of the gate centered on the top of the echo. By changing the width of the gate, either nonselective detection which collects responses from all the signals within the excitation bandwidth of the microwave pulses or a selective detection which virtually eliminates the contribution from off-resonance signals is chosen. In the echo-detected EPR, the intensity of Hahn echo (90°—τ—180°—τ—echo) was measured as a function of the external magnetic-field strength *B*. By using a selective detection, the resolution similar to that of cw EPR is attained. For the pulsed ENDOR measurement, Mims sequence[14] in which radiofrequency pulse (duration 10 μs) was inserted between the second and the third pulses of stimulated echo (90°—τ—90°—T—180°—τ—echo, τ =1.2 μs, T=16 μs) was used.

III. EXPERIMENTAL RESULTS AND ANALYSIS

In all P-doped 3*C*-, 4*H*-, and 6*H*-SiC CVD layers, the photoluminescence (PL) of the P-bound excitons has been observed. Figure 1 shows as an example the band-edge PL spectrum in a 6*H*-SiC layer with strong no-phonon lines and phonon replicas of the P-bound excitons measured in the configuration with the electromagnetic waves of photons polarized perpendicular to the *c* axis ($\mathbf{E}\perp\mathbf{c}$). Detailed structures of the spectra were reported elsewhere.[13,15] The *R* and *S* no-phonon lines of the N-bound excitons were also detected but very weak. The observation of the strong PL of P-bound excitons indicates the high purity of our CVD layers. [In the sublimation-grown material, the PL of the P-bound excitons was usually not seen and only the broad PL band from the donor-acceptor pairs was detected (Ref. 10).] In our 3*C*-, 4*H*-, and 6*H*-SiC CVD samples, the EPR signals of the shallow N donors were not observed.

A. EPR spectra and hyperfine interaction

1. 6*H*-SiC

Figures 2(a) and 2(b) show the *W*-band (~95 GHz) EPR spectra in P-doped 6*H*-SiC measured at 6 K for the magnetic field **B** along and perpendicular to the *c* axis, respectively. The spectrum consists of two doublets, each due to ^{31}P hyperfine structure. We will show later in Sec. V that these doublets correspond to the shallow P donors occupying the two quasicubic lattice sites of silicon and therefore give the P_1 and P_2 spectra new labels P_{k1} and P_{k2}, respectively. The observed ^{31}P hf splitting are P_{k1} (0.11 mT) and P_{k2} (0.615 mT) at $\mathbf{B}\|\mathbf{c}$ and P_{k1} (not resolved) and P_{k2} (0.22 mT) at $\mathbf{B}\perp\mathbf{c}$. From the symmetry ($C_{3v}$), the *g* values and the ^{31}P hf constants shown in Table I, it is concluded that these doublets are identical to the P_1 and P_2 spectra in Refs. 2 and 5 or the I_1 and I_2 spectra in Ref. 4.

As shown in $\times 10$ scale spectrum in Fig. 2(b), a weak satellite line on the low-field side of the P_{k1} line could be detected. The intensity ratio between this satellite line and the main P_{k1} line is about 0.6% which is approximately a half of the natural abundance of ^{13}C (I=1/2, 1.1%). This satellite is therefore attributed to the low-field component of the ^{13}C hf structure of the C atom along the *c* axis in the nearest-neighbor shell. Within the experimental error, the ^{13}C hf splitting (~0.37 mT$\times$2=0.74 mT) was isotropic.

In the *X*-band EPR spectra of P-doped 6*H*-SiC at 8 K, three doublets P_{k1}, P_{k2a}, and P_{k2b} are observed as shown in

TABLE I. The principal values of g and hf tensors of the shallow P donors in 3*C*-, 4*H*-, and 6*H*-SiC. The error in the g values is ±0.0002. The values of the hf splitting are given in mT. The values in parentheses are in MHz. The principal g values were determined from *X*-band and *W*-band cw EPR.

Center	$g_{\parallel}$	$g_{\perp}$	$A_{\parallel}(^{31}\mathrm{P})$	$A_{\perp}(^{31}\mathrm{P})$	$A_{\parallel}(\mathrm{C}_1)$	$A_{\perp}(\mathrm{C}_1)$	$A_{\parallel}(C_{2\text{-}4})$	$A_{\perp}(\mathrm{C}_{2-4})$	
P (3*C*)	2.0051	2.0046	(0.53)[a]	(−0.13)[a]					
P_k(4*H*)	2.0065	2.0006	0.294 [c,d]	0.21[c,d]	0.72[e]	0.72[e]			
			(8.24)[c,d]	(5.89)[c,d]	(20.18)[e]	(20.18)[e]			
P_{k1}(6*H*)	2.0046	2.0028	0.11[d]	0.01[d]	0.74[c]	0.74[c]			
			(3.168)[a]	(0.0654)[a]	(20.7)[c]	(20.7)[c]			
P_{k2}(6*H*)	2.0039	2.0025	0.619[d]	0.22[d]	1.09[c]	1.09[c]	1.09[c]	~0.61[c]	~0.61[c]
			0.615[c]	0.22[c]	(30.6)[c]	(30.6)[c]	(17.1)[c]	(17.1)[c]	
			(17.012)[a,b]	(6.155)[a,b]					

[a]Determined from pulsed ENDOR with a higher accuracy.
[b]Determined from pulsed ESEEM with a higher accuracy.
[c]Determined from *X*-band cw EPR.
[d]Determined from *W*-band cw EPR.
[e]Determined from *X*-band echo-detected EPR.

Fig. 3. At $\mathbf{B}\|\mathbf{c}$ [Fig. 3(a)], two doublets P_{k1}, P_{k2a} are observed. With rotating the magnetic field away from the c axis, the intensity of the P_{k2a} doublet rapidly decreases while the P_{k2b} doublet appears and dramatically increases. For the intermediate directions (between 20° and 70°), all the P_{k1}, P_{k2a}, and P_{k2b} doublets can be seen [see Fig. 3(b)], whereas at $\mathbf{B}\perp\mathbf{c}$, the P_{k2b} doublet reaches its maximum intensity and the P_{k2a} signal is not detectable [Fig. 3(c)]. The ^{31}P hf splitting of the P_{k1} and P_{k2} doublets observed at *W* band agree with those of P_{k1} (0.11 mT) and P_{k2a} (0.619 mT) at *X* band for $\mathbf{B}\|\mathbf{c}$ and with those of P_{k1} (not resolved) and P_{k2b} (0.22 mT) at *X* band for $\mathbf{B}\perp\mathbf{c}$.

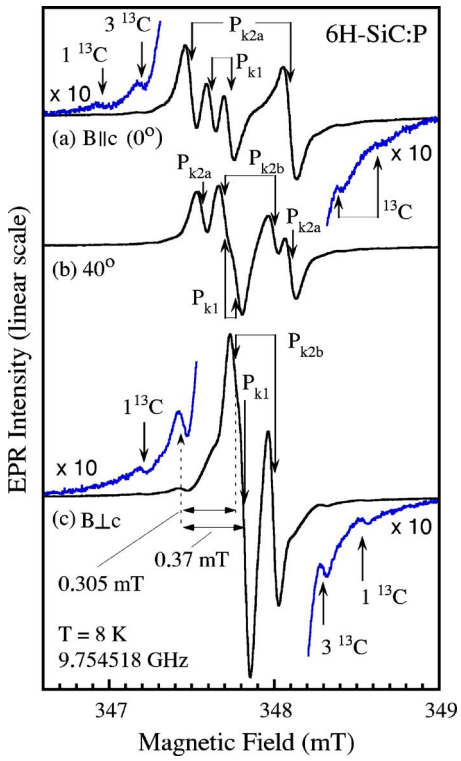

FIG. 3. (Color online) *X*-band EPR spectra in P-doped 6*H*-SiC freestanding layers measured at 8 K for (a) $\mathbf{B}\|\mathbf{c}$, (b) $\mathbf{B}$ is 40° from the c axis and (c) $\mathbf{B}\perp\mathbf{c}$. The scaled-up spectra show the ^{13}C hf lines of nearest-neighbor C atoms.

As shown in the ×10 scale, two pairs of satellite lines centered at the P_{k2a} signal were also detected for some angles close to the c axis [Fig. 3(a)]. The outer pair has a nearly isotropic splitting of ~1.09 mT and the intensity ratio between the sum of the outer pair of the satellite lines and the main line is about 0.9–1.3 % which corresponds to the natural abundance of ^{13}C. The outer satellites are therefore attributed to the ^{13}C hf lines of one nearest-neighbor C atom along the c axis (C_1). The intensity ratio between the sum of the inner pair of the satellite lines and the main line is about 2.7–3.4%. The inner satellites with a nearly isotropic splitting of ~0.61 mT are therefore assigned to be the ^{13}C hf lines of three nearest-neighbor C atoms in the basal plane (C_{2-4}). The anisotropy of these hf splitting is too small to be detected with the resolution of cw EPR. Two sets (outer and inner pairs) of ^{13}C satellites with both the hf splitting and the intensity relative to the main line similar to those of the P_{k2a} doublets were also detected for the P_{k2b} doublets for the directions close to $\mathbf{B}\perp\mathbf{c}$ [Fig. 3(c)]. A better analysis of the intensity ratio was possible, confirming that these hf lines are due to the interaction with one and three C atoms in the nearest-neighbor shell. The intensity of the inner hf line on the low-field side in Fig. 3(c) is much higher than expected for the hf interaction with three C nuclei on the P_{k2b} line. This is due to the overlapping between the inner hf line of P_{k2b} (with a half hf splitting ~0.305 mT) and the outer hf line of the P_{k1} line with a half hf splitting of ~0.37 mT as determined from the *W*-band experiments [see Fig. 2(b)].

Figures 4(a) and 4(b) show the pulsed-ENDOR spectra of the P_{k1} center measured for $\mathbf{B}\|\mathbf{c}$ and $\mathbf{B}\perp\mathbf{c}$, respectively. For $\mathbf{B}\perp\mathbf{c}$, the P_{k1} line overlaps with the low-field component of the P_{k2b} doublet in the *X*-band EPR spectrum and therefore ENDOR frequencies from both doublets, P_{k1} and P_{k2b}, were detected [Fig. 4(b)]. The angular dependence of the ENDOR lines of P_{k1} with $\mathbf{B}$ rotating in the $(1\bar{1}00)$ plane is shown to

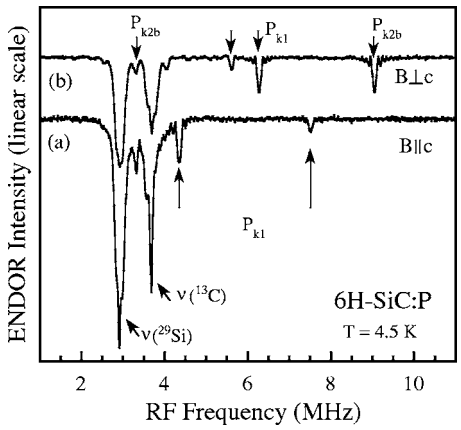

FIG. 4. ENDOR spectra in P-doped 6*H*-SiC measured for (a) $\mathbf{B}\|\mathbf{c}$ and (b) $\mathbf{B}\perp\mathbf{c}$. The magnetic field was set on the P_{k1} EPR peak.

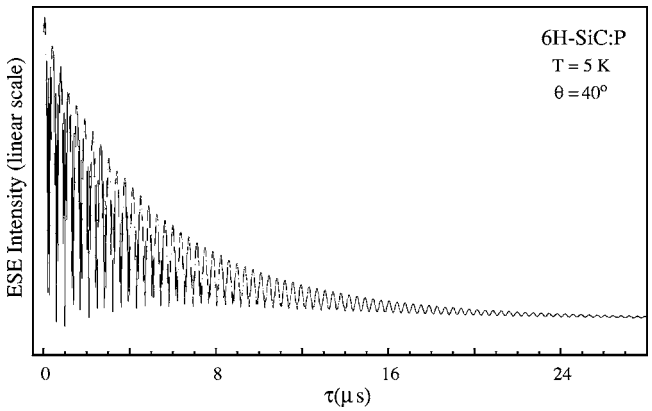

FIG. 5. Two-pulse ESEEM time-domain spectrum of the P_{k2a}/P_{k2b} doublets in P-doped 6*H*-SiC measured at 5 K for **B** being 40° off the *c* axis.

have axial symmetry and therefore can be described by the following equation:[16]

$$\nu_{\mathrm{ENDOR}}(M_S = \pm 1/2) = \{[(\pm 1/2)(A_\parallel \sin^2\theta + A_\perp \cos^2\theta) - \nu(^{31}\mathrm{P})]^2 + [(A_\parallel - A_\perp)\sin\theta\cos\theta]^2\}^{1/2}. \quad (1)$$

Here M_S is the magnetic quantum number of the electron spin, ν (^{31}P) is the nuclear Zeeman frequency of ^{31}P corresponding to the applied magnetic field, and the angles $\theta = 0°$ and $\theta = 90°$ correspond to the directions $\mathbf{B}\|\mathbf{c}$ and $\mathbf{B}\perp\mathbf{c}$, respectively. The ^{31}P hf constants obtained from the least-squares fitting of the observed ENDOR frequencies of P_{k1} by using Eq. (1) are given in Table I and are in good agreement with the values determined for the P_1 center in Refs. 2 and 5.

There is a remarkable difference in the signal intensity and its angular variation of the P_{k2} doublet measured at different frequencies. At 142 GHz, the intensity of the P_2 signal was found to be double as compared to that of P_1 and was therefore attributed to the unresolved spectra originated from two P centers occupying the two quasicubic sites (k_1, k_2) of 6*H*-SiC lattice.[2,4,5] In our *W*-band (~95 GHz) experiments, the intensity of the P_{k2} doublet is comparable to or smaller than that of the P_{k1} signal (see Fig. 2). This does not support the assignment of the P_2 doublet in Ref. 2. At high frequencies (95 and 142 GHz), the change of the signal intensity with the crystal directions is small and completely different from the strong intensity variation of the P_{k2a} and P_{k2b} doublets measured at *X*-band frequency. At the directions between 40° and 60°, the separation between the P_{k2a} and P_{k2b} lines in the *X*-band spectra is about 0.10–0.11 mT. However, in the P_{k2} lines of the *W*-band spectra (the line width ~0.1 mT), no indication of an overlapping of two signals such as splitting or broadening could be detected. We therefore suspect that the P_{k2a} and P_{k2b} doublets seen in *X*-band experiments are not related to two different P centers as previously suggested[2,4–6,12] but may be corresponding to allowed ($\Delta M_S = \pm 1$, $\Delta m_I = 0$, here m_I is the magnetic quantum number of the nuclear spin) and forbidden transitions ($\Delta M_S = \pm 1$, $\Delta m_I = \pm 1$) of one P center with $S = 1/2$, $I = 1/2$. This may happen for a system with an anisotropic hf interaction, which is comparable in magnitude to the nuclear Zeeman interaction, when the direction of the hf field is different from that of the external magnetic field. In such a case, ESEEM arising from the interference between allowed and forbidden transitions, which are excited simultaneously by microwave pulses, may be observable.[17]

Figure 5 shows the two-pulse echo decay spectrum measured at 5 K for the magnetic field direction being 40° off the *c* axis. In the measurement, the intensity of Hahn echo (90°—τ—180°—τ—echo) was measured as a function of the interpulse delay τ by using the microwave pulses sufficiently strong to excite all four lines of the P_{k2a}/P_{k2b} doublets simultaneously and by using nonselective detection. As can be seen in the figure, a very strong modulation on the two-pulse echo decay was observed. In the two-pulse ESEEM experiment, the modulation frequencies are the ENDOR frequencies, $\nu_\alpha[\nu_{\mathrm{ENDOR}}(M_S = +1/2)]$ and $\nu_\beta[\nu_{\mathrm{ENDOR}}(M_S = -1/2)]$, and the combination frequencies, $\nu_\alpha \pm \nu_\beta$ (Ref. 18). After subtracting the slow decay due to the spin-relaxation processes, the time-domain spectrum (Fig. 5) is converted to the frequency-domain spectrum by Fourier transformation (FT). In the FT-ESEEM spectrum shown in Fig. 6, the first and the third frequencies (lines 1 and 3) correspond to the ENDOR frequencies whereas lines 2 and 4

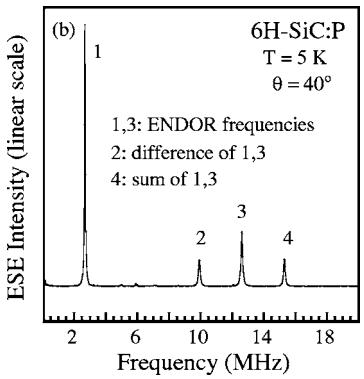

FIG. 6. Two-pulse ESEEM frequency-domain spectrum of the P_{k2a}/P_{k2b} doublets in P-doped 6*H*-SiC measured at 5 K for **B** being 40° off the *c* axis.

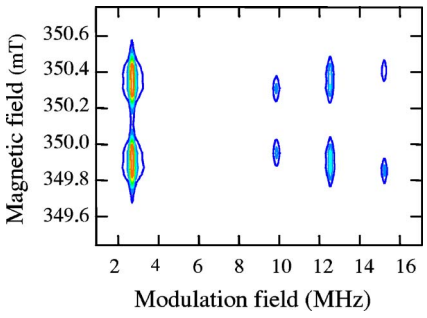

FIG. 7. (Color online) A 2D-EPR spectrum showing the contour plot of the modulation intensities with respect to the modulation frequency and the magnetic field measured at the same angle as in Fig. 6 (**B** is 40° off the *c* axis).

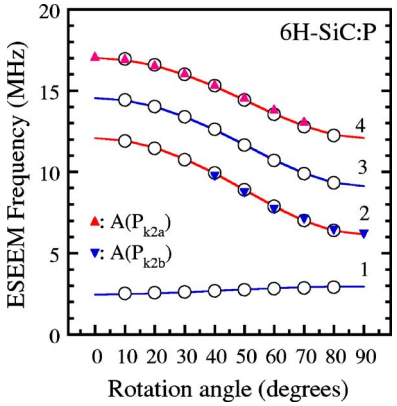

FIG. 8. (Color online) Angular dependences of ENDOR frequencies (1 and 3), their difference and sum (2 and 4) obtained from ESEEM (open circles) and the hf splitting obtained from cw EPR of the P_{k2a} and P_{k2b} doublets (filled triangles) in 6*H*-SiC. The solid curves are calculated from the obtained hf parameters using Eq. (1).

correspond to the difference and the sum of the frequencies 1 and 3, respectively.

In the ESEEM experiment, only one set of ENDOR frequencies was obtained from the four lines of the P_{k2a}/P_{k2b} doublets. The sorting of the four lines of the two doublets, P_{k2a} and P_{k2b}, to the allowed transitions ($\Delta m_I=0$) and formally forbidden transitions ($\Delta m_I=\pm 1$) of a center with $S=1/2$ and $I=1/2$ is clearly demonstrated by using the 2D-EPR technique.[18] In our 2D-EPR experiment, the time-sweep mode spectra, echo intensity versus τ, of the Hahn echo were measured as a function of the external magnetic-field strength B at the same orientation as the above ESEEM experiment, i.e., 40° off the *c* axis. All four lines of the P_{k2a}/P_{k2b} doublets were excited by strong microwave pulses and a selective detection was used to extract the modulation from the particular EPR transition. For the latter purpose, the echo intensity was obtained by integrating the echo shape sampled in the range of 400 ns with a step of 4 ns. The FT-ESEEM spectra as a function of B were obtained by converting each time domain spectrum to the frequency domain spectrum. Figure 7 shows a contour plot of the modulation intensities with respect to the two axes: the modulation frequency and the magnetic field. The ^{31}P ENDOR frequencies of 2.7 and 12.6 MHz are observed at the field positions of both P_{k2a}/P_{k2b} doublets. The difference of the ENDOR frequencies 9.9 MHz occurs only at the field positions of the P_{k2b} doublet (~349.95 and ~350.3 mT), while the sum of the ENDOR frequencies 15.3 MHz occur only at the field positions of the P_{k2a} doublet (349.85 and 350.4 mT). Thus the P_{k2a}/P_{k2b} doublets are clearly arising from one P center with $S=1/2$, $I=1/2$. Although being excited by the microwave pulses, the P_{k1} doublet does not give any modulation and therefore gives rise to no peaks in the 2D-EPR spectrum in Fig. 7.

The angular dependence of the modulation frequencies with **B** rotating in the $(1\bar{1}00)$ plane is shown in Fig. 8. The modulation was not observed at 0° ($\mathbf{B}\|\mathbf{c}$) and 90° ($\mathbf{B}\perp\mathbf{c}$) since at these principal directions of the ^{31}P hyperfine tensor (C_{3v} symmetry), the $\Delta m_I=\pm 1$ transitions should have zero transition probability. In Fig. 8, the splitting of the P_{k2a} and P_{k2b} doublets in the *X*-band cw-EPR spectra is also plotted. The splitting of the P_{k2a} and P_{k2b} doublets corresponds very well to the fourth (line 4) and second (line 2) modulation frequencies, respectively. This confirms that the two doublets P_{k2a} and P_{k2b} belong to the same P center with $S=1/2$ and $I=1/2$. The angular dependence of the ENDOR frequencies (lines 1 and 3) were fitted using Eq. (1) and the principal values of the ^{31}P hf tensor, $A_{\|}=17.012$ MHz and $A_{\perp}=6.155$ MHz, were obtained. The same values of the hf constants were also obtained from the least-squares fitting of the second and fourth modulation frequencies, $\nu_\alpha-\nu_\beta$ and $\nu_\alpha+\nu_\beta$. It should be noted that the ^{31}P hf tensor obtained from the angular dependence of the ESEEM frequencies agrees with that obtained for the P_{k2} center from the *W*-band cw-EPR measurements. Thus the four lines of the P_{k2a}/P_{k2b}doublets are arising from the P_{k2} center. The simulation of the angular dependences of the ESEEM frequencies using the obtained hf coupling constants are plotted as solid curves in Fig. 8.

The relative intensities between the P_{k2a} and P_{k2b} doublets change with the direction of the magnetic field indicates that their associated transitions change from allowed to forbidden transitions and vice versa. This happens in the case when the hf interaction is anisotropic and comparable in strength with the nuclear Zeeman interaction. Figure 9 shows the energy-level scheme for $S=1/2$ and $I=1/2$ and the allowed and

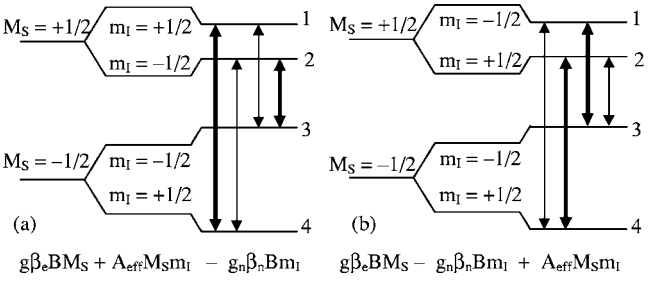

FIG. 9. Energy-level scheme for a system with $S=1/2$, $I=1/2$ for the cases (a) $A_{eff}>2g_n\beta_nB>0$, and (b) $2g_n\beta_nB>A_{eff}>0$. Here M_S and m_I are the magnetic quantum numbers of the electron and nuclear spins, respectively. The equations of the energy for the case of high magnetic field and isotropic hf interaction is valid only at the principal directions of the hf tensor (see text for explanation).

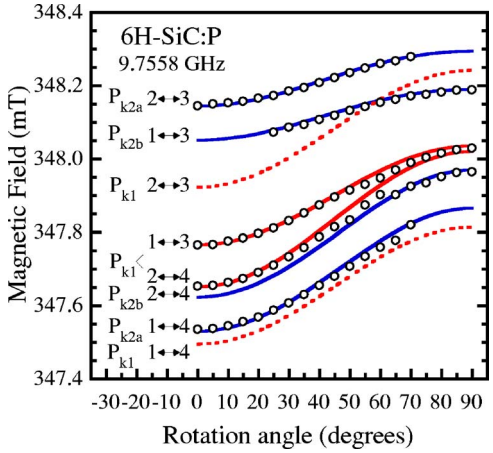

FIG. 10. (Color online) The angular dependences of the line positions of P centers in 6*H*-SiC measured at *X*-band frequency (9.7558 GHz) with **B** rotating in the $(1\bar{1}00)$ plane. The curves represent the calculated line positions for all possible EPR transitions of P_{k1} and P_{k2} centers using the parameters in Table I and the spin Hamiltonian Eq. (2). For the P_{k2} center, all the EPR transitions become allowed or partly allowed and can be detected at most of crystal directions. For the P_{k1} center, the transitions $(1\leftrightarrow4)$ and $(2\leftrightarrow3)$ corresponding to the outside lines (dashed curves) are not detectable.

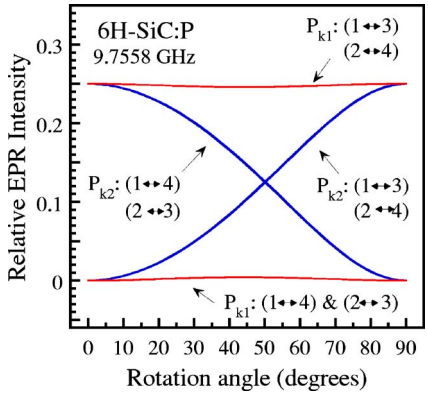

FIG. 11. (Color online) Angular dependence of the relative EPR intensity of all the transitions of the P_{k1} and P_{k2} centers in 6*H* -SiC calculated at *X*-band frequency (9.7558 GHz). At *W*-band frequencies, the intensity dependence of both the P_{k1} and P_{k2} centers is similar to that of the P_{k1} center at *X*-band frequency.

forbidden transitions depending on the magnitude of the hf coupling constant and the nuclear Zeeman interaction. The levels are split by the electron Zeeman interaction $g\beta_e BM_S$, the hf term $A_{eff}M_S m_I$ and the nuclear Zeeman term $-g_n\beta_n Bm_I$ ($A_{eff}>0$, $g_n>0$). Here β_e and β_n are the Bohr magneton and nuclear magneton, respectively. It should be noticed that the simple equation $(g\beta_e BM_S+A_{eff}M_S m_I-g_n\beta_n Bm_I)$ for the case of high magnetic field and isotropic hf interaction is only valid at the principal directions of the hf tensor of P_{k2} and is used for an easy understanding of the energy-level scheme. For an arbitrary direction of the magnetic field, the energy levels are described by more complicated terms.[19] Figure 9(a) shows the case for $A_{eff}>2g_n\beta_n B$. The allowed transitions $1\leftrightarrow4$ and $2\leftrightarrow3$ (indicated as thick arrows) are determined by the selection rule $\Delta M_S=\pm1$ and $\Delta m_I=0$. For $A_{eff}<2g_n\beta_n B$, the transitions $2\leftrightarrow4$ and $1\leftrightarrow3$ become allowed as shown in Fig. 9(b). When the anisotropic hf interaction is comparable to the nuclear Zeeman interaction, the selection rules are relaxed and all four transitions may be detectable. The intensity of the forbidden transitions is determined by both the relative magnitude between the anisotropic hf coupling constants and $g_n\beta_n B$ and the relative direction between the anisotropic hf and **B**.

The angular dependences of the P_{k2} doublet (P_{k2a} and P_{k2b} doublets) in 6*H*-SiC measured with **B** rotating in the $(1\bar{1}00)$ plane are plotted as open circles in Fig. 10. The spin Hamiltonian parameters **g** and **A** of ^{31}P, both having C_{3v} symmetry, were determined by fitting the observed line positions of *X*-band measurements to the spin Hamiltonian

$$H=\beta_e\mathbf{B}\cdot\mathbf{g}\cdot\mathbf{S}+\mathbf{S}\cdot\mathbf{A}\cdot\mathbf{I}-g_n\beta_n\mathbf{B}\cdot\mathbf{I}, \qquad (2)$$

where $S=1/2$ and $I=1/2$, and $g_n=2.2632$ for ^{31}P. The least-squares fitting of the line positions and the calculations of the transition probabilities to be described later were carried out by computer program EPR.FOR using numerical diagonalization of the spin-Hamiltonian matrix. The principal *g* and *A* values of the P_{k2} centers obtained are given in Table I. The analysis of the angular dependence of the line positions measured at *W*-band frequency gives the same principal *g* values and similar ^{31}P hf coupling constants for P_{k2}. Our *g* values are about 0.0003 smaller than that reported in Refs. 2 and 5 and are close to the values given in Ref. 6. In our experiments, the magnetic field was calibrated by measuring simultaneously the signals arising from the substitutional P in Si ($g=1.9985$, isotropic) in P-doped Si which was co-mounted with the P-doped SiC sample. The simulated angular dependences of these doublets using the obtained values and the spin Hamiltonian Eq. (2) are plotted as solid and dashed curves in Fig. 10. The angular dependences of the relative intensity of all the four EPR transitions are calculated and shown in Fig. 11. If we assume that the P_{k2a} and P_{k2b} doublets were arising from two different centers and obtain the spin-Hamiltonian parameters from the line positions observed for the limited range of the orientations, the obtained parameters ($g_\parallel=2.0039$, $g_\perp=2.0025$, $A_\parallel=0.615$ mT, $A_\perp=0.43$ mT for P_{k2a} and $g_\parallel=2.0038$, $g_\perp=2.0025$, $A_\parallel=0.396$ mT, $A_\perp=0.22$ mT for P_{k2b}) correspond well to those of dP_{c1} ($g_\parallel=2.0037$, $g_\perp=2.0025$, $A_\parallel=0.62$ mT, $A_\perp=0.38$ mT) and dP_{c2} ($g_\parallel=2.0037$, $g_\perp=2.0024$, $A_\parallel=0.48$ mT, $A_\perp=0.19$ mT), respectively.[6]

From Figs. 10 and 11, it is clear that at both *X*-band and *W*-band frequencies and for all crystal directions the P_{k1} center follows the energy-level scheme in Fig. 9(b) and only two allowed transitions $2\leftrightarrow4$ and $1\leftrightarrow3$ can be detected. The two forbidden transitions $1\leftrightarrow4$ and $2\leftrightarrow3$ have nearly zero transition probability and cannot be observed (dashed curves in Fig. 10). Therefore the hyperfine patterns of the P_{k1} spectra at *X* band and *W* band are similar. The situation of the P_{k2} center is, however, different. In the case of the P_{k2} center at *X*-band frequency, the ^{31}P hf interaction is larger than $2g_n\beta_n B$ for the crystal directions between 0° and ~50°, and therefore splitting follows the scheme in Fig. 9(a) in which the $1\leftrightarrow4$ and $2\leftrightarrow3$ transitions are allowed. Between ~50°

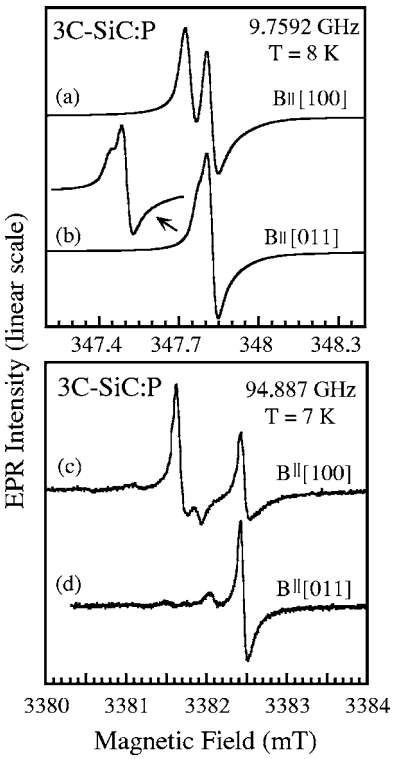

FIG. 12. *X*-band EPR spectra in P-doped 3*C*-SiC CVD layers measured at 8 K for (a) $\mathbf{B}\|[100]$ and (b) $\mathbf{B}\|[011]$. The inset shows the spectrum in (b) measured with a four-time-smaller field modulation (0.005 mT). The microwave power is ~0.006 mW. (c), and (d) The corresponding spectra measured at *W*-band frequency, respectively.

and 90°, the ^{31}P hf interaction is smaller than $2g_n\beta_nB$ and the energy levels are described by the scheme in Fig. 9(b) in which the $2\leftrightarrow4$ and $1\leftrightarrow3$ transitions become allowed. At directions between 20° and 70°, all four EPR transitions can be detected (Fig. 11). The analysis of the angular dependence of the P_{k2} center at *W*-band frequency shows that at higher magnetic fields (nearly ten times compared to that at *X*-band frequency), the hf term is much smaller than $2g_n\beta_nB$ at all directions. The system therefore follows the energy-level scheme in Fig.9(b) and only the transitions $2\leftrightarrow4$ and $1\leftrightarrow3$ can be detected. The calculations also show that the angular variation of the intensity of the P_{k2} signal at *W*-band frequency is similar to that of the P_{k1} center.

2. 3C-SiC

Figures 12(a) and 12(b) show the *X*-band EPR spectra observed in a P-doped 3*C*-SiC CVD freestanding film at 8 K for $\mathbf{B}\|[100]$ and $\mathbf{B}\|[011]$, respectively. For $\mathbf{B}\|[100]$, a spectrum with two lines was detected. These two lines coincide at $\mathbf{B}\|[111]$ and move away from each other when rotating to the [011] direction. At $\mathbf{B}\|[011]$, these lines almost overlap with each other and can be slightly resolved when using low microwave power (0.006 mW) and low-field modulation (0.005 mT) [see the inset in Fig. 12(b)]. The corresponding spectra measured at *W*-band frequency are shown in Figs. 12(c) and 12(d). From *X*-band to *W*-band frequency, the splitting between the two lines at $\mathbf{B}\|[100]$ increases nearly ten times, indicating that the separation between the two lines is not due to the hf splitting but due to the difference in the *g* value. The angular dependence of the line positions with **B** rotating in the $(0\bar{1}1)$ plane was measured at both *X*-band and *W*-band frequencies and shown in Figs. 13(a) and 13(b), respectively. The center has two magnetically distinguishable sites both at $\mathbf{B}\|[100]$ and at $\mathbf{B}\|[011]$, and only one at $\mathbf{B}\|[111]$. From the pattern of the rotational plots shown in Fig. 13, it is determined that the symmetry of the center is D_{2d}. Thus the center has three sites which are axially symmetric about [100], [010], and [001], respectively. The line positions of two sites of which the symmetry axes are [010] and [001], respectively are identical in the rotation with $\mathbf{B}\perp[0\bar{1}1]$. From the least-squares fitting of the line positions observed, the same principal values, $g_\parallel=2.0051$, $g_\perp=2.0046$, of the *g* tensor (with D_{2d} symmetry) were obtained for both rotations. The simulations of the line positions using the obtained parameters are plotted as solid curves in Fig. 13.

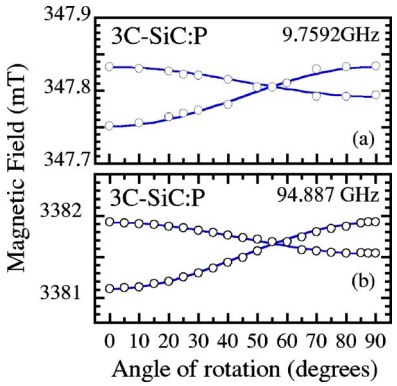

FIG. 13. (Color online) Angular dependence of the line positions of the P center in 3*C*-SiC measured at (a) 9.7592 GHz and (b) 94.887 GHz with **B** rotating in the $(0\bar{1}1)$ plane. The curves represent the calculated line positions using the parameters in Table I. The angles 0° and 90° corresponding to the magnetic-field directions $\mathbf{B}\|[100]$ and $\mathbf{B}\|[011]$, respectively.

In order to extract weak ^{31}P hyperfine interaction hidden underneath the linewidth, we performed pulsed-ENDOR experiments. Figures 14(a) and 14(c) show the pulsed-ENDOR spectra for $\mathbf{B}\|[100]$ and $\mathbf{B}\|[011]$ with the magnetic field fixed at the EPR line position of the site which is axially symmetric about [100]. For both directions, two ENDOR lines centered at $\nu(^{31}\mathrm{P})$ were detected. For $\mathbf{B}\|[100]$, the separation of the two ENDOR lines was the same as Fig. 14(c) when the magnetic field was fixed at the high-field EPR line arising from the two sites which are axially symmetric about [010] and [001], respectively. The angular dependence of the ENDOR lines in the $(0\bar{1}1)$ plane shown in Fig. 14(b) indicates that the ^{31}P hf tensor is axially symmetric about the ⟨100⟩ direction. From the least-squares fitting of the angular dependence of the ENDOR frequencies to Eq. (1), we obtain the principal values of the hf tensor $A_\parallel=0.53$ MHz and $A_\perp=-0.13$ MHz. The ^{31}P hf tensor has also D_{2d} symmetry. The principal values are very small and the hyperfine splitting changes the sign when passing the ⟨111⟩

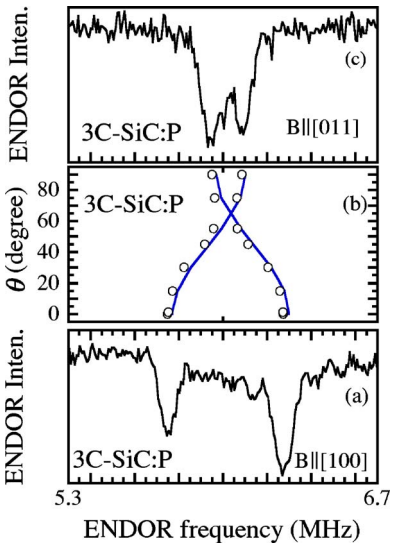

FIG. 14. (Color online) ENDOR spectra and the angular dependence of ENDOR frequencies of the P center in 3*C*-SiC. The angles $\theta=0°$ and $\theta=90°$ correspond to the directions $\mathbf{B}\|[100]$ and $\mathbf{B}\|[011]$, respectively. The solid curves in (b) represent the fit using the hf parameters in Table I.

direction. Since the pulsed-ENDOR measurements confirm that the center is related to P, the center is labeled the P center.

3. 4H-SiC

In 4*H*-SiC layers doped with P during CVD growth, an EPR doublet was detected. The *X*-band spectra measured at 8 K for $\mathbf{B}\|\mathbf{c}$ and $\mathbf{B}\|\mathbf{c}$ are shown in Figs. 15(a) and 15(b), respectively. Although there are two inequivalent silicon sites (*h* and *k*) in 4*H*-SiC, only one spectrum was detected in both *X*-band and *W*-band experiments. We label the spectrum as P_k and the assignment of the center to P at the *k* site will be shown later. For $\mathbf{B}\perp\mathbf{c}$ or angles between 60° and 90° a satellite line was observed on the high-field side of the P_k line [see the inset in Fig. 15(b)]. Its intensity ratio with the main line is about 0.5–0.6 %, indicating that the structure is due to the high-field component of the ^{13}C hf structure of the C atom along the *c* axis in the nearest-neighbor shell. Similar to the hf line of P centers in 6*H*-SiC, this hf splitting is also isotropic. The low-field component of the hf structure could not be detected due to overlapping with a broad and isotropic signal at ~347.8 mT [see Fig. 15(b)]. For angles close to the *c* axis, the P_k signal becomes weaker and the ^{13}C hf structure could not be observed. In *W*-band EPR experiments, the broad signal is well separated from the P signal, but we could not detect the ^{13}C hf lines as clear as in *X*-band experiments.

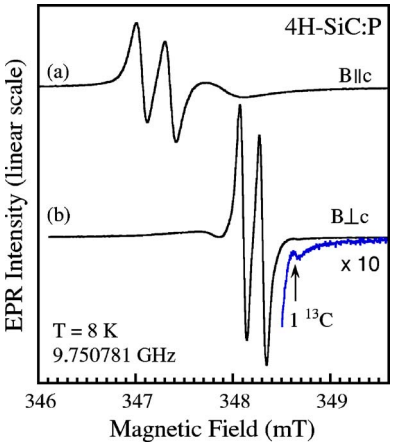

FIG. 15. (Color online) EPR spectra in P-doped 4*H*-SiC freestanding layers measured at 8 K for (a) $\mathbf{B}\|\mathbf{c}$ and (b) $\mathbf{B}\perp\mathbf{c}$. The isotropic broad signal at ~347.85 mT is not related to the P_k center. The ^{13}C hf line of one nearest-neighbor C atom could be detected for the high-field line of the ^{31}P doublet.

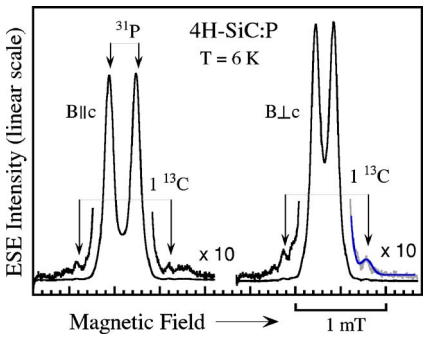

FIG. 16. (Color online) *X*-band echo-detected EPR spectra of P_k in 4*H*-SiC measured at 6 K for **B** along and perpendicular to the *c* axis showing the hf structure of ^{31}P. The ^{13}C hf lines of one C atom is also observed and shown in ×10 scale parts of the spectra.

In Fig. 16, echo-detected EPR spectra of P_k in 4*H*-SiC measured for $\mathbf{B}\|\mathbf{c}$ and $\mathbf{B}\perp\mathbf{c}$ are shown. In the echo-detected EPR spectra the broad signal was effectively eliminated by utilizing the difference in the phase memory time which is the time constant of the two-pulse echo decay. As can be seen in the ×10 scale spectra in Fig. 16, weak hf lines similar to that in cw-EPR spectra could be detected. Within the experimental error, the hf splitting is isotropic(~0.72 mT). The intensity ratio between the hf line and the main line is also about 0.5–0.6 %. A part of the simulated spectrum including the hf interaction with one ^{13}C nucleus plotted as a smooth curve at the high-field side of the P_k line at $\mathbf{B}\perp\mathbf{c}$ shows an excellent fit to the experimental data (the grey curve underneath). This confirms that the satellite lines are due to the ^{13}C hf interaction with one nearest-neighbor C atom, which we assign to be the nearest C atom along the *c* axis. The hf interaction with three nearest-neighbor C atoms in plane was not resolvable from the main line.

From the angular dependence of the line positions shown in Fig. 17, it is determined that the symmetry of the P_k center is C_{3v}. In Fig. 17, each open circle represents an EPR line position measured in the *X*-band spectra and the solid curves are the simulated angular dependence using the EPR parameters (see Table I) obtained by fitting of the observed line positions to the spin Hamiltonian Eq. (2). The analysis shows that at both *X*-band and *W*-band frequencies, the nuclear Zeeman interaction is larger than the hf interaction and the splitting follows the scheme in Fig. 9(b). Only the transitions $2\leftrightarrow4$ and $1\leftrightarrow3$ corresponding to the inner doublet can be detected. The calculations of the relative intensity show that

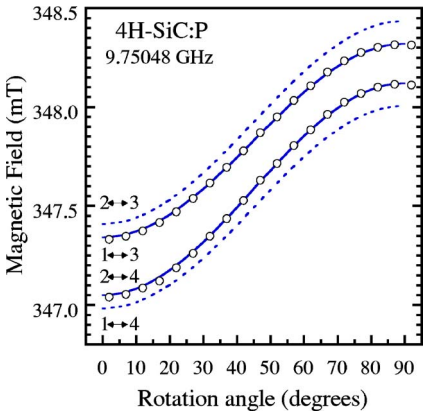

FIG. 17. (Color online) Angular dependence of the P_k center in 4*H*-SiC measured at 9.75048 GHz with **B** rotating in the $(1\bar{1}00)$ plane. The curves represent the calculated line positions of all the four possible EPR transitions of the P_k center ($S=1/2$ and $I=1/2$) using the parameters in Table I and the spin Hamiltonian of Eq. (2). The dashed curves represent the transitions with the intensity close to zero and cannot be detected. The relative intensity of the transitions is similar to that of the P_{k1} center in 6*H*-SiC shown in Fig. 11.

the transitions $1 \leftrightarrow 4$ and $2 \leftrightarrow 3$ (dashed curves in Fig. 17) are forbidden and could not be detected in our *X*-band and *W*-band experiments.

4. LCAO analysis

Since the hf interactions of ^{31}P and ^{13}C have either axial symmetry or isotropic we can estimate the isotropic and anisotropic parts of the hf tensor and hence the corresponding *s* and *p* spin densities using one-electron linear-combination-of-atomic-orbital (LCAO) approximation. The isotropic part is the trace of tensor **A** and is related to the spin density in the *s* orbital ($\eta^2\alpha^2$) by the expression

$$a = 1/3(A_{\parallel} + 2A_{\perp}) = (2/3)\mu_0 g\beta_e g_n \beta_n \eta^2 \alpha^2. \quad (3)$$

The anisotropic part is the traceless part of an axial tensor with principal values $(2b,-b,-b)$, where *b* is expressed via the spin density in the *p* orbital ($\eta^2\beta^2$) as

$$b = (1/3)(A_{\parallel} - A_{\perp}) = (2/5)(\mu_0/4\pi) g\beta_e g_n \beta_n \eta^2 \beta^2 \langle r^{-3}\rangle_p. \quad (4)$$

Here, η^2 is the spin density on the corresponding atom and the contribution of the *d* orbital was not considered ($\alpha^2+\beta^2=1$). The obtained hf values *a* and *b* for P centers in 3*C*-, 4*H*-, and 6*H*-SiC are given in Table II. The spin densities on the *s* and *p* orbitals then can be calculated using atomic constants, $|\psi(0)|^2$ and $\langle r^{-3}\rangle_p$, given by Morton and Preston.[20] The obtained spin densities at the P atom and the nearest-neighboring C atom(s) are also shown in Table II.

B. Temperature dependence of signal intensity and spin-lattice relaxation time

Below we show that the P centers in 3*C*-SiC, P_k in 4*H*-SiC, and P_{k1} and P_{k2} in 6*H*-SiC exhibit features characteristic of having a low-lying excited state. The energy separation between the ground state and the excited state has been estimated from the temperature dependence of the cw-EPR signal intensity and of the spin-lattice relaxation time. Later, after assigning the P centers to be the shallow donors, the splitting is ascribed to valley-orbit splitting.

TABLE II. The hf parameters *a* and *b* and the corresponding *s* and *p* spin densities of the unpaired electron located on the P atom and their nearest-neighbor C atoms. The anisotropic part of ^{13}C hf interaction which could not be resolved by cw-EPR measurements was assumed to be 0. The total spin density for $C_{2\text{-}4}$ is the triplex value of the sum $(s+p)$.

Center	*a* (MHz)	*b* (MHz)	*s* (%)	*p* (%)	Total (%)
P (3*C*)					
^{31}P	0.09	0.22	0.0007	0.06	0.06
P_k (4*H*)					
^{31}P	6.67	0.78	0.05	0.21	0.26
C_1	20.18	0	0.53	0	0.53
P_{k1} (6*H*)					
^{31}P	1.492	0.838	0.01	0.23	0.24
C_1	20.7	0	0.55	0	0.55
P_{k2} (6*H*)					
^{31}P	9.774	3.169	0.07	0.86	0.93
C_1	30.6	0	0.81	0	0.81
$C_{2\text{-}4}$	17.1	0	0.45	0	1.35

In our studies of the temperature dependence of the cw-EPR signals, the measurements were performed at *W*-band frequency using very low microwave powers to achieve the stability in coupling of microwave in the cavity. The temperature dependence of the EPR signal of the P center in 3*C*-SiC, P_k and P_{k1} in 4*H*-, and 6*H*-SiC is very similar as can be seen in Fig. 18. The signal gradually decreases with increasing temperature and disappears at temperatures above 30–34 K. The P_{k2} doublet in 6*H*-SiC behaves differently and can be detected only at temperatures below 12 K [see Fig. 18(c)].

Here, we consider a simple model consisting of only two states, the ground state and the excited state with the energy difference ΔE, by neglecting higher excited states and the conduction-band states. The temperature dependence of the EPR signal intensity of the ground state is given for the case of ΔE which is much larger than the Zeeman splitting δ,

$$I_0(T) \propto n_0(T) f(T). \quad (5)$$

The temperature dependence of the population of the ground state due to thermal excitation to the excited state is

$$n_0(T) = N[g_0/(g_0+g_1)\exp(-\Delta E/k_B T)], \quad (6)$$

where *N* is the concentration of the EPR center, g_0 and g_1 are the degeneracy without including electron spin of the ground state and excited state, respectively, and k_B is the Boltzmann constant. The fraction excess population of the lower level of the electron Zeeman levels is

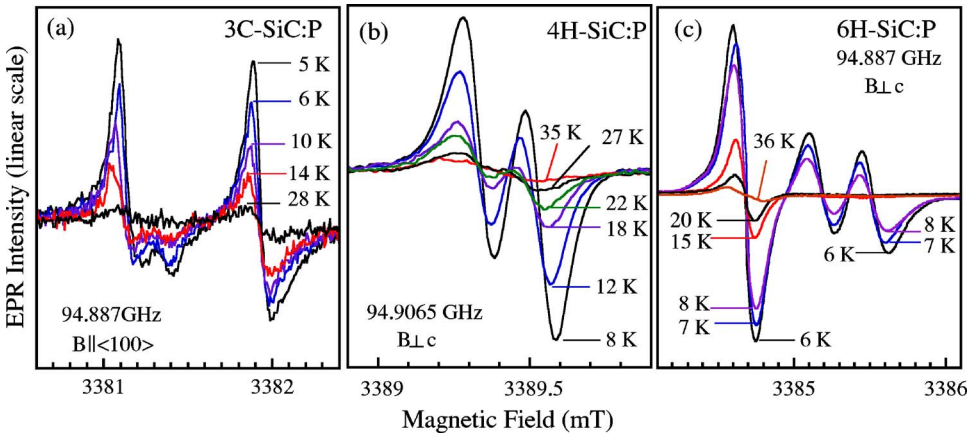

FIG. 18. (Color online) Temperature dependence of the P centers in (a) 3*C*-, (b) 4*H*-, and (c) 6*H*-SiC. EPR measurements were performed at *W*-band for (a) $\mathbf{B}\|\langle 100\rangle$ and (b), (c) $\mathbf{B}\perp\mathbf{c}$.

$$f(T) = [1 - \exp(-\delta/k_B T)]/[1 + \exp(-\delta/k_B T)] = \tanh(\delta/2k_B T), \quad (7)$$

where $\delta \sim 0.39$ meV at the *W*-band frequency. The calibrated intensities of the P center in 3*C*-SiC, P_k in 4*H*-SiC and P_{k1}, P_{k2} centers in 6*H*-SiC are plotted as a function of the reciprocal temperature in Fig. 19. The fits to the EPR intensities using Eqs. (5)–(7) are also shown as solid curves in Fig. 19. The energy separation ΔE determined for the P centers are 5.4 meV for 3*C*-SiC, 4.8 meV for P_k in 4*H*-SiC, 4.2 meV, and 7.0 meV for P_{k1} and P_{k2} in 6*H*-SiC, respectively.

The energy separation between the ground state and the excited state can also be determined from the temperature dependence of the spin-lattice relaxation time T_1 in the temperature range where T_1 is governed by the Orbach process which is the resonant two-phonon process involving an actual excited energy level lying at ΔE above the studied level.[21] In this process, the temperature dependence of T_1 is described by the relation

$$1/T_1 \propto \exp(-\Delta E/k_B T). \quad (8)$$

For measuring T_1 we performed inversion-recovery experiments in which a pulse sequence $(180°-t-90°-\tau-180°-\tau-\text{echo})$ with fixed τ and scanned t was used. The first pulse creates a nonequilibrium population. The Hahn echo generated by the second and third pulses monitors the recovery to the thermal equilibrium population.

Below 10 K, the inversion-recovery curves of the P-related centers in 4*H*- and 6*H*-SiC could be well fitted by a single exponential function. The temperature dependence of T_1 measured for $\mathbf{B}\perp\mathbf{c}$ is shown in Fig. 20 for P_k in 4*H*-SiC and for P_{k1} and P_{k2} in 6*H*-SiC. As can be seen in the figure, the logarithm of $1/T_1$ in both polytypes is linear to the reciprocal of the temperature with the slope determined by an energy separation ΔE. The obtained ΔE values are 4.2 meV for P_k in 4*H*-SiC, 4.3 meV and 6.0 meV for P_{k1} and P_{k2} in 6*H*-SiC, respectively. These values are in good agreement with those determined from the temperature dependence of the cw-EPR signal intensity.

It should be noted that ΔE is obtained from the measurement of T_1 in the low-temperature region where the decrease of the signal intensity due to the population onto the excited state is not significant. One of the main sources of errors in the determination of the energy separation via the temperature dependence of T_1 comes from the measurement of temperature. In the studied temperature range 5–10 K, a small error in measuring temperature, e.g., 0.5–1 K, would result

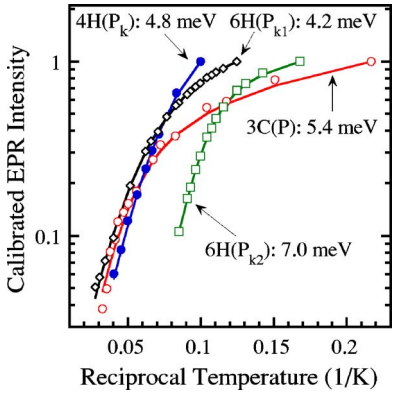

FIG. 19. (Color online) Calibrated EPR intensity of the P signals in 3*C*-, 4*H*-, and 6*H*-SiC as a function of reciprocal temperature. The deduced energy separations between the ground and excited states of the P-related centers are indicated. The solid curves represent the fits using Eqs. (5)–(7). The data were obtained from *W*-band experiments.

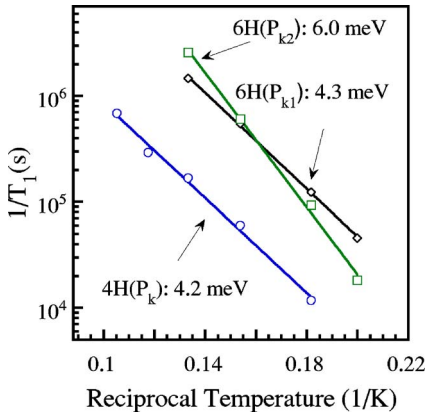

FIG. 20. (Color online) The dependence of the spin-lattice relaxation time T_1 on the reciprocal temperature of P centers in 4*H*-SiC and 6*H*-SiC. The solid lines represent the fits to experimental data. The corresponding energy separations between the ground and excited state of P centers are indicated.

in an error of ~0.6–1.0 meV in ΔE. In cw-EPR experiments, the ΔE values of the P center in 3*C*-SiC, P_k in 4*H*-SiC, and P_{k1} in 6*H*-SiC were determined in a larger temperature range (6–30 K) and were therefore less sensitive to the temperature error. In our *W*-band experiments, the sample and the cavity are in contact with a thick copper holder, where the temperature sensor is attached, and the temperature can be kept stable within 0.05 K during the measurement. The temperature stability in our *X*-band spectrometer is also similar. However, the temperature sensor mounted outside of the resonator for the pulse experiments and its reading could be slightly different from the real temperature of the sample which is in a small quartz tube inside the resonator. We expect that the error in measuring temperature can be ~0.5 K and less than 1 K in both *X*-band and *W*-band experiments.

In the T_1 measurements of P in 3*C*-SiC, the obtained inversion recovery curves at the studied temperatures could not be fitted to a single exponential function. For successful estimation of ΔE from measurements of T_1, P-doped 3*C*-SiC samples with higher quality and lower doping may be required (our P-doped 3*C*-SiC CVD layers were grown in the conditions optimized for 4*H*- and 6*H*-SiC but not for the 3*C* polytype).

IV. CALCULATIONS

A. Methodology

Ab initio supercell calculations were carried out to investigate the shallow phosphorus donor at the Si site in 4*H*-SiC. The donor wave function can spread out large distance from the donor atom in semiconductors. By using the effective-mass state theory the radii of the donor wave function associated with the ground state can be estimated to be 11 Å.[22] We have used a 576-atom supercell ($6\times6\times2$ multiplication of the primitive cell) to model the 4*H*-SiC crystal where the average diameter of this supercell is somewhat bigger than 20 Å. (Here, we note that $6\times6\times2$ multiplication of the 6*H*-SiC primitive cell would result in a 864-atom supercell.) In a small supercell the donor wave function can strongly overlap with its periodic images. This is manifested by the accumulation of the localization of donor wave function at the edge of the supercell. We have inspected the localization of the donor wave function at the edge of the 576-atom supercell and we have not found any peaks. Therefore we believe that the calculated spin distribution in this supercell can be qualitatively compared to the experimental values. (We note that the donor wave functions of the excited states may spread out at larger distances, therefore the inaccuracy of the calculation could be larger for the excited states.) The effective-mass donor states are split off from the conduction-band states at the edge of the conduction bands. The minimum of the conduction-band edge (CBM) of 4*H*-SiC is at the *M* point.[23] In order to study the shallow donors in 4*H*-SiC, the donor wave functions should be calculated at the *M* point. In the above-mentioned 576-atom supercell calculations the *M*-point is folded into the Γ point of the reduced Brillouin zone of this large supercell. Since the Γ-point sampling provides convergent charge density in an 576-atom supercell[24] we have used this single *k* point only in the calculations.

The calculation on defects in a 576-atom supercell (even with a single *k* point) at *ab initio* level is computationally almost prohibitive but it is possible by using supercomputers. We have used the parallel version of the code SIESTA[25] to accomplish this task. This program implements density functional theory (DFT) combined with the pseudopotential approximation to eliminate the core electrons, and uses a basis set consisting of numerical orbitals centered on the atoms. In the calculations of P_{Si} defects Troullier-Martins pseudopotentials were employed.[26] The program requires the use of a grid to compute some of the contributions to the matrix elements and also for performing the Fourier transform to evaluate the Hartree potential and energy by solving the Poisson's equation in reciprocal space. We have used a grid fine enough to represent plane waves with kinetic energy cutoff up to 90 Ry. A high quality basis set was used, consisting of double-ζ plus polarization functions for the valence electrons. These calculations have been carried out using the Ceperley-Alder functional[27] as parametrized by Perdew and Zunger.[28] We have used spin polarized calculation but it was beyond of our possibility to take the spin-orbit interaction into account. We have used the scissor operator to correct the "band-gap" error of this method. In order to optimize the geometry of the donors the forces acting on the atoms have to be calculated which is computationally demanding. To accelerate this process we have first optimized the defects in a smaller 96-atom supercell and insert the resulting geometry into the large 576-atom supercell. Then, those atoms were again post-relaxed in the 576-atom supercell until the forces were below 0.04 eV/Å. Since we have used pseudopotentials to treat core electrons a direct calculation of hyperfine constants of the paramagnetic defect is beyond the possibility. However, the spin localization on P and nearest-neighboring C atoms can be calculated by this method and compared to the values derived from experiments.

B. Results

We have investigated P occupying the Si site at both hexagonal (*h*) and cubic (*k*) lattice sites in 4*H*-SiC. We have found that the relaxation effect is relevant in the first two neighbor shells around P atom: the distance between the first neighbor C atoms and P atom is shortened to 1.82–1.83 Å while the bond length between the second neighbor Si atoms and first neighbor C atoms is stretched to 1.91 Å. In the outer shells the bond lengths are practically identical to those in the perfect crystal (1.88 Å). We do not find significant difference in the geometry of $P_{Si}(k)$ or $P_{Si}(h)$ defects: $P_{Si}(k)$ is somewhat more symmetric possessing bond length of 1.82 Å between P and every neighbor C atom while $P_{Si}(h)$ has 0.01 Å longer P-C bond along the *c* axis. The calculated donor level at *k* site (P_k) is at E_C-17 meV with A_1 symmetry where E_C is the conduction-band edge. (We note here that we obtained this symmetry without applying the spin-orbit coupling.) The calculated first excited *E* state is lying 8 meV higher in energy. The situation is different at the *h* site (P_h): the ground state has *E* symmetry with the level at

E_C-19 meV while the first excited A_1 state is lying above only with 4 meV. We have to note here that the LDA Kohn-Sham levels are not the ionization energies. One can have a reasonable value for the ionization energies by using the so-called ΔSCF method, i.e., the energy difference between the neutral state and the ionized (single positively charged) state. By using this method we have obtained the vertical ionization energies at E_C-76 meV/56 meV for the k/h sites, respectively. These values are close to the ionization energy of 60.7 meV for P at the k site determined recently from fitting the donor-acceptor luminescence due to Al-P pairs.[29] As a check, we have calculated the vertical ionization energies of N donors. The obtained values at E_C-142/44 meV should be compared to the recently measured ones at $\sim E_C$ -125 meV/61 meV (Refs. 29 and 30) at k/h sites, respectively. The N donors have a nondegenerate ground state following by the E state at both sites in agreement with the experiment. We note that these values are also close to the recently reported thermal ionization energies calculated in a smaller supercell.[31]

Based on these results we can say that both P_k and P_h are shallower than the $N_C(k)$ donor in 4H-SiC. For P_h the difference between energies of the E and A_1 states are very small. We could not check whether the order of the levels would change in a bigger supercell. Nevertheless, we could look at the trend by using a smaller supercell. In a 96-atom supercell (its average diameter is about 5 Å) the A_1 state of P_h is deeper by 101 meV than the E state. (The level of the A_1 state is at E_C-128 meV in the 96-atom supercell because of the over localization of the donor state due to the relatively small size of the supercell.) This means that by increasing the supercell size the E state becomes more stable than the A_1 state for P_h. The difference between the A_1 and E states also slightly decreases for P_k but the former one remains the ground state in the large supercell. We incline to claim that the ground state of P_k is nondegenerate while the ground state of P_h has E symmetry. Still, the energy difference is small for both sites. Therefore we have calculated the localization and the corresponding s,p,d character of the donor wave function for both the A_1 and E states. The results are summarized in Table III. As can be seen in Table III, the d component is relatively big on the P atom. It is not unexpected because the d orbitals of the silicon atoms contribute significantly to the lowest conduction-band state.

TABLE III. The localization and s, p, d character of the donor wave function at different sites in 4H-SiC obtained by the *ab initio* supercell calculations. The *total* spin density for $C_{2\text{-}4}$ is the triplex value of the sum $(s+p+d)$.

Center/ symmetry	s (%)	p (%)	d (%)	Total (%)
P_k/A_1				
P	0.05	0.70	0.46	1.21
C_1	0.88	0.01	0.00	0.89
$C_{2\text{-}4}$	0.00	0.00	0.00	0.00
P_k/E				
P	0.00	0.16	0.37	0.53
C_1	0.00	0.00	0.00	0.00
$C_{2\text{-}4}$	0.02	0.07	0.00	0.27
P_h/E				
P	0.00	0.31	0.80	1.11
C_1	0.00	0.00	0.02	0.02
$C_{2\text{-}4}$	0.70	0.03	0.00	2.19
P_h/A_1				
P	0.16	0.21	0.75	1.12
C_1	0.07	0.16	0.00	0.23
$C_{2\text{-}4}$	0.14	0.02	0.00	0.48

V. DISCUSSION

In all the studied 3C-, 4H-, and 6H-SiC samples, only the P-related EPR centers were observed whereas the EPR signal of the N donors was not detectable. In our P-doped 4H- and 6H-SiC layers, the concentration of P measured by SIMS (Ref. 13) correlates well with the donor concentration determined by current-versus-voltage (CV) measurements, indicating that P introduced into the layer during CVD growth acts as shallow donors. This is also supported by the observation of strong PL emissions of the P-bound excitons in our 4H- and 6H-SiC CVD layers. The PL lines in 3C-SiC samples are broad and it is difficult to separate the lines belonging to N-bound excitons and/or to P-bound excitons. The 3C-SiC layers are more conducting compared to the 4H- and 6H-SiC samples. Since the EPR signal of the N donor was not detected, we believe that P is responsible for the conductivity of the 3C-SiC layers.

The observation of the ^{31}P hyperfine interaction provided evidence that P is involved in the centers. The P_k center in 4H-SiC and the P_{k1} and P_{k2} centers in 6H-SiC exhibit the ^{31}P hyperfine structure in their cw-EPR spectra. The involvement of ^{31}P in the P_{k1} and P_{k2} centers in 6H-SiC was previously identified by ENDOR,[2,5] and also confirmed by our pulsed-ENDOR and ESEEM experiments. The involvement of ^{31}P in the P center in 3C-SiC is confirmed by pulsed-ENDOR.

The detection of the ^{13}C satellite lines in the EPR spectra in 4H- and 6H-SiC elucidates that carbon atom(s) is/are the nearest neighbor(s) and P substitutes for Si. The low concentration of both intrinsic defects and common impurities such as N in our CVD layers enabled us to observe weak satellite lines arising from the ^{13}C hf interaction with nearest-neighboring C atom(s). From the covalent radii (0.77 Å for C, 1.11 Å for Si, and 1.06 Å for P), it is natural to assume that P resides at the Si site. In previous studies of P in neutron-transmuted 6H-SiC,[1–6] P was assumed to occupy the Si site since the neutron irradiation transmutes ^{30}Si to ^{31}P on site. Therefore the P_1/P_2 (P_{k1}/P_{k2} in our notation) and the P_a/P_b centers[2,5] were all assigned to the shallow P donors at the Si site although no hf structure due to the interaction with neighboring C atoms was observed. However, recent theoretical studies[9] pointed out that P doped by neutron transmutation is incorporated favorably into the carbon sublattice through kinetic effects during the high-temperature annealing process which is required for the activation of the P donors.

The P_a/P_b centers are assigned to P at the C site or a pair of P at the C site and a carbon antisite (C_{Si}), $P_C C_{Si}$.[9] In our samples of 6*H*-SiC doped with P during CVD growth, only the P_{k1}/P_{k2} spectra were detected and the P_a/P_b centers were not observed. In 3*C*-SiC, no direct evidence, such as the hf structure due to the interaction with the nearest neighbors, indicating the site occupation of the P center was observed. However, it is reasonable to expect that the introduction of P into 3*C*-SiC lattice during CVD growth is similar to that into 4*H*- and 6*H*-SiC and P also substitutes for Si.

The observed EPR centers are not likely to be a pair of P and a V_C, P_{Si}-V_C. In our samples, we could not detect any EPR signals of the silicon vacancy (V_{Si}^-) and the carbon vacancy (V_C^+), which can be seen sometimes in substrates grown by high-temperature CVD or by sublimation technique. The near-infrared PL of the silicon vacancy[32] was also not detected. We therefore believe that in our CVD films the concentration of vacancies must be a few orders of magnitude less than that of P. This is also supported by recent *first principles* calculations of P doping in 4*H*-SiC,[31] in which the concentration of complexes between P and vacancies is predicted to be four to five orders of magnitude less than the total P concentration in equilibrium. The involvement of V_C in the P-related dP_h, dP_{c1}, and dP_{c2} centers (or P_{k1} and P_{k2} centers in our notation) in 6*H*-SiC as previously suggested[6] is therefore unlikely. The model of P_{Si}-V_C pairs was based on the observation of satellite lines which were attributed to ^{29}Si hf of two equivalent neighboring Si atoms.[6] The splitting of these satellite lines corresponds to the ^{13}C hf lines of one neighboring carbon atom in our spectra. In Ref. 6, the intensity ratio between the satellites and the main line was obtained by fitting the line shape with assuming the overlapping of three spectra of N, dP_h, and dP_{c2} centers. It is likely that their determination of the intensity of very weak satellite lines were hampered by the presence of N ($\sim 1.2 \times 10^{16}$ cm^{-3}) and possibly other intrinsic defects in the P-doped samples by neutron transmutation using the neutron dose as high as 1×10^{20} cm^{-2}. Another argument against the model of the P_{Si}-V_C pairs is that only the centers with C_{3v} symmetry which matches the vacancy at the nearest carbon site along the *c* axis were detected and no C_{1h}-symmetric centers which should be expected for the configuration with the vacancy at the nearest carbon site of one of three basal carbon atoms could be seen.

These EPR centers exhibit the temperature dependence of the signal intensities due to the presence of a low-lying excited state which is attributed to the valley-orbit splitting. We have estimated the valley-orbit splitting also from the temperature dependence of the spin lattice relaxation time.[33] There are three equivalent conduction-band minima (valleys) in 3*C*-SiC in which the conduction-band minimum is at the *X* point of the Brillouin zone. In the effective-mass approximation, the hydrogen-atom-like 1*s* ground state of the shallow donors has threefold degeneracy due to the three conduction-band minima. Under the T_d symmetry of the donor site, the 1*s* ground state either remains threefold degenerate with a triplet state T_2 or splits into a singlet state A_1 and a doublet state *E*. The symmetry of the P center in 3*C*-SiC is lowered to D_{2d}. A T_2 state under the T_d symmetry gives a singlet state B_2 and a doublet *E*. An *E* state under the $T_d$symmetry splits into a singlet state B_1 and a singlet state A_1. In 4*H*-SiC in which the conduction-band minimum is located at the *M* point, the threefold degeneracy of the 1*s* ground state is split into a singlet state A_1 and a doublet state *E* under the C_{3v} symmetry of the donor site. In 6*H*-SiC in which the conduction-band minimum lies along the *M*-*L* line, the sixfold degeneracy of the 1*s* ground states splits into two singlets A_1 and two doublets *E* under the C_{3v} symmetry of the donor site. While the other hydrogenlike excited states $(2p_0, 2s, 2p_\pm, \ldots)$ lie well above these 1*s* states, the separation between the 1*s* states (valley-orbit splitting) is rather small. Thus the intensity of the EPR signal arising from the donor electrons bound in the ground state of the valley-orbit splittingdecreases with the increase of the temperature according to the thermally excited population on the low-lying excited state. In the PL studies of P-doped 6*H*-SiC,[15] a feature associated with the Ph^c no-phonon line was assigned to be related to the valley-orbit level lying at 5.2 and 6 meV above the ground level. In a recent electronic Raman study, Püsche and co-workers[34] determined the valley-orbit splitting for P centers to be 2.2 and 4.3 meV for 4*H*-SiC, 3.5 and 5.3 meV for 6*H*-SiC. These values are close to ours (4.2/4.3 meV for P_{k1} and 7.0/6.0 meV for P_{k2}). As temperature increases, not only the relative population of the excited state increases but also the jumping rate between the ground and the excited states increases. If the excited state was independently observed, the EPR parameters should be different from those of the donor ground state. Thus the jumping between the ground and excited states causes line broadening unless averaging is achieved. The presence of the low-lying excited state provides an efficient spin-lattice relaxation process known as Orbach process which contributes to line broadening as the temperature increases. At higher temperatures, a certain fraction of the donor electrons are thermally excited into the conduction band. The exchange scattering between the donor electrons and the conduction electrons might also cause the line broadening.[35] With these mechanisms ofthe line broadening, EPR spectra of donors are observable only at relatively low temperatures.

Since the isotropic part of the ^{31}P hf interaction of the P center in 3*C*-SiC is very small, it is likely that the donor electron wave function has a node at the phosphorus nucleus. Thus the ground state of the P center in 3*C*-SiC is likely to be originated from the *E* state or the T_2 state under T_d symmetry. As described above, the twofold degeneracy of the *E* state is split into A_1 and B_1 and the threefold degeneracy of the T_2 state is split into a singlet B_2 and a doublet *E* under the D_{2d} symmetry. Thus the nondegenerate ground state (B_1 or B_2 under the D_{2d} symmetry) is achieved by the tetragonal distortion in the P center in 3*C*-SiC. Our theoretical studies for the P occupying the Si site in 4*H*-SiC has suggested that the ground state of the *h* site should be a doublet *E* while the ground state of the *k* site should be a singlet A_1. The assignment of the P_k spectrum to the *k* site is also supported by the calculations of the localization of the donor wave function. As shown in Table III, the spin densities on the P atom and on the nearest-neighbor carbon atoms are calculated for both A_1 and *E* states of both *k* and *h* sites. The 576-atom supercell might be not large enough to make a direct comparison be-

tween the theoretical values and the experimental data. Since the localization of the donor wave function decays at the edge supercell, the results obtained in this supercell may be used qualitatively. It can be seen that the calculated localization on the P atom is somewhat overestimated compared to the experiments which could be due to the supercell size. Nevertheless, only the spin density of the A_1 ground state of the k site fits the experimental data of the P_k center in which only one set of ^{13}C satellites corresponding to the interaction with one C atom has been observed. In all the other combinations, the localization on three carbon neighbors ($C_{2\text{-}4}$) is much stronger than that on one carbon neighbor (C_1), which is in contradiction with the experimental findings.

The results of calculations in 4*H*-SiC may be not transferable to the polytype of 6*H*-SiC because of two reasons: (i) the CBM in 6*H*-SiC is along the *M*-*L* line[36] and not at the *M* point as in the 4*H*-SiC therefore the character of the donor wave function can differ, (ii) the radii of the donor wave function is around 11 Å while the lattice constant of 6*H* -SiC along the *c* axis is around 15 Å. This means that the donor wave function "feels" locally the 6*H*-SiC environment differently from that in the 4*H* polytype.

In previous studies,[2,5] the P_2 doublet in 6*H*-SiC was believed to be the coincidence of two different P spectra from the 1:2 intensity ratio between the P_1 and P_2 doublets measured at 142 GHz. It was therefore naturally to assign the P_2 doublet (P_{k2} in our notation) to be related to P at two quasicubic sites in 6*H*-SiC and the P_1 doublet (P_{k1} in our notation) to P at the *h* site. The assignment was supported by recent calculations,[9] which predicted well the hf coupling constants for P_1 (P_h) and P_2 (with nearly the same hf splitting for P at the k_1 and k_2 site). However, as shown in the previous section, the P_{k2a}/P_{k2b} doublets indeed belongs to allowed and forbidden transitions of the P_{k2} center, and therefore the P_2 doublet is not contributed from two different P centers with similar *g* value and hf splitting as previously suggested.[2,5,9,12] It is reasonable to assume that the properties of P centers at two quasicubic sites may be similar and can be quite different from that of the P center at the *h* site. If P at one of the two quasicubic sites is detected, one would expect to observe also the EPR spectrum belonging to P at the other quasicubic site. In 6*H*-SiC, only two P-related spectra were detected. It is therefore likely that these two spectra belong to P at the two quasicubic sites and the missing spectrum is related to the P donor at the hexagonal site, P_h. The P_k center in 4*H*-SiC is indeed similar to the P_{k1} center in the 6*H* polytype in temperature dependence and the spin localization on the P donor and surrounding C atoms. In the electronic Raman study by Püsche and co-workers,[34] the P centers in 4*H*-SiC have the valley-orbit splitting of 2.2 and 5.3 meV. In 6*H*-SiC, only two Raman lines corresponding to the valley-orbit splitting of 3.5 and 5.3 meV were observed in the whole energy range between 10 cm^{-1} (~1.24 meV) and 2000 cm^{-1} (~247.97 meV).[34] The valley-orbit splitting corresponding to the third P center in 6*H*-SiC may be smaller than 10 cm^{-1} so that the Raman line is too close to the laser line and is technically not detectable. The missing of the EPR signal of P at the *h* site in both 4*H*- and 6*H*-SiC is likely to be related to the *E* ground state whose degeneracy is not lifted under the site symmetry of C_{3v} or the energy separation between the A_1 and *E* states is very small (~2.2 meV or less, Ref. 34). The degenerate or near-degenerate ground state is sensitive to local strains and the EPR spectrum might easily be broadened beyond observation.

In the recent EPR study of *in situ* P-doped 6*H*-SiC by sublimation technique,[9] besides the strong signal of the N donors, only the fingerprint of the P+*V* center was believed to be detected (as weak shoulders of the central line of N spectrum). Therefore it was concluded that in the P-doped samples during sublimation growth the amount of electrically active isolated P is not significant and P may mainly form complexes, which may be in diamagnetic states and could not be detected by EPR. However, our studies show that P incorporated during CVD growth substitutes for Si and acts as shallow donors. The formation of P-related complexes during the growth if occurred should be a minor process and the concentration of P-related complexes is insignificant compared to that of the isolated shallow P donors. We believe that in the P-doped sublimation samples the signals of the shallow P donors are obscured by the strong signal of the N donors.

VI. SUMARY

In summary, we have observed P-related EPR spectra in 3*C*- (P center), 4*H*- (P_k center), and 6*H*-SiC (P_{k1} and P_{k2} centers) doped with P during CVD growth. All the centers are identified to be related to the ground state of the shallow P donors at the Si site. From the *g* anisotropy, it is determined that the P_k center in 4*H*-SiC and the P_{k1} and P_{k2} centers in 6*H*-SiC have C_{3v} symmetry and the P center in 3*C*-SiC has D_{2d} symmetry. The central ^{31}P hf interaction is resolved in cw EPR for the P_k center in 4*H*-SiC and the P_{k1} and P_{k2} centers in 6*H*-SiC and is extracted by ENDOR for the P center in 3*C*-SiC. The ^{31}P hf interaction of the P_{k1} and P_{k2} centers in 6*H*-SiC is confirmed by ENDOR. The ^{13}C satellite line(s) of the nearest-neighboring C atom(s) which are evidence that the P atom occupies the Si sublattice are observed for the P_k center in 4*H*-SiC and the P_{k1} and P_{k2} centers in 6*H*-SiC. The valley-orbit splitting of these shallow P donors were determined from the temperature dependence of the intensity of cw-EPR signals and of the spin-lattice relaxation time. In 3*C*-, 4*H*-, and 6*H*-SiC, the obtained valley-orbit splitting are in the range 4–7 meV and close to the value determined from electronic Raman studies in 4*H*- and 6*H*-SiC and from PL spectra of the P bound excitons in 6*H*-SiC.

The P_{k1} and P_{k2} centers in 6*H*-SiC were found to be identical to the EPR doublets P_1, P_2 (or dP_h, dP_1, and dP_2) which were previously reported in neutron transmuted material. Our ESEEM results show that the previously reported dP_1 and dP_2 doublets observed in *X*-band EPR or the P_2 doublet measured at high frequencies are not originated from two different P centers occupying two inequivalent quasicubic silicon sites of 6*H*-SiC lattice but belong to allowed and forbidden transitions of one P center, P_{k2}, with $S=1/2$ and $I=1/2$. The analysis of the angular dependence including the nuclear Zeeman interaction provides a satisfactory explana-

tion of the angular dependence of the intensity of the P_{k2} doublet in6*H*-SiC. The ESEEM and new ENDOR data provide a more precise determination of the hf coupling constants of the shallow P donors in 6*H*-SiC.

Comparing spin densities on the P atom and surrounding C atoms determined by EPR experiments and by *ab initio* supercell calculations, we assign the P_k center in 4*H*-SiC to the A_1 ground state of the shallow P donor occupying the quasicubic site. Expecting that the P centers at the two quasicubic sites have similar properties, which can be quite different from that of the P donor at the hexagonal site, we attribute the P_{k1}, P_{k2} centers in 6*H*-SiC to the shallow P donors at the k_1 and k_2 quasicubic sites. The missing EPR spectrum in both 4*H*- and 6*H*-SiC is ascribed to the shallow P donor at the hexagonal site P_h with the degenerate or near-degenerate *E* ground state. From the identification of P centers at the silicon site in 4*H*- and 6*H*-SiC CVD layers, it is expected that P introduced into 3*C*-SiC during CVD growth also occupies the silicon site.

ACKNOWLEDGMENTS

The computer program EPR.FOR was developed by the group of Professor J. A. Weil, University of Saskatchewan. Support for this work by the Swedish Foundation for Strategic Research (SSF) program SiCMAT and by the Grant-in-Aid for Scientific Research in Priority Areas "Semiconductor Nanospintronics" (Grant No. 16031202) of the Ministry of Education, Culture, Sports, Science, and Technology, Japan, is acknowledged. Support by the Hungarian OTKA F-038357, and Grant No. 2005008 from the Swedish National Supercomputer Center are appreciated. We are grateful to Dr. N. Mizouchi for the help in the analysis of 2D-EPR.

[1] M. Laube, F. Schmid, G. Pensl, G. Wagner, M. Linnarsson, and M. Maier, J. Appl. Phys. **92**, 549 (2002).
[2] S. Greulich-Weber, Phys. Status Solidi A **162**, 95 (1997), and references therein.
[3] A. I. Veinger, A. G. Zabrodskii, G. A. Lomakina, and E. N. Mokhov, Fiz. Tverd. Tela **28**, 1659 (1984); [Sov. Phys. Solid State **28**, 917 (1986)].
[4] E. N. Kalabukhova, S. N. Lukin, and E. N. Mokhov, Fiz. Tverd. Tela **35**, 703 (1993); [Phys. Solid State **35**, 361 (1993)].
[5] E. N. Kalabukhova, S. N. Lukin, E. N. Mokhov, M. Feege, S. Greulich-Weber, and J -M. Spaeth, Inst. Phys. Conf. Ser. **137**, 215 (1994).
[6] P. G. Baranov, I. V. Ilyin, E. N. Mokhov, H. J. von Bardeleben, and J. L. Cantin, Phys. Rev. B **66**, 165206 (2002).
[7] J. Isoya, T. Ohshima, A. Ohi, N. Morishita, and H. Itoh, Nucl. Instrum. Methods Phys. Res. B **206**, 965 (2003).
[8] J. Isoya, T. Ohshima, N. Morishita, T. Kamiya, H. Itoh, and S. Yamasaki, Physica B **340-342**, 903 (2003).
[9] E. Rauls, M. V. B. Pinheiro, S. Greulich-Weber, and U. Gerstmann, Phys. Rev. B **70**, 085202 (2004).
[10] M. V. B. Pinheiro, S. Greulich-Weber, and J. -M. Spaeth, Physica B **340-342**, 146 (2003).
[11] K. Semmelroth, F. Schmid, D. Karg, G. Pensl, M. Maier, S. Greulich-Weber, and J. -M- Spaeth, Mater. Sci. Forum **433-436**, 63 (2003).
[12] N. T. Son, A. Henry, J. Isoya, and E. Janzén, Mater. Sci. Forum **483-485**, 515 (2005).
[13] A. Henry and E. Janzén, Mater. Sci. Forum **483-485**, 101 (2005).
[14] W. B. Mims, Proc. R. Soc. London, Ser. A **238**, 452 (1965).
[15] S. G. Sridhara, L. L. Clemen, D. G. Nizhner, R. P. Devaty, W. J. Choyke, and D. J. Larkin, Mater. Sci. Forum **264-268**, 465 (1998).
[16] A. Schweiger and G. Jeschke, in *Principles of Pulse Electron Paramagnetic Resonance*, (Oxford University Press, New York, 2001), p. 58.
[17] L. G. Rowan, E. L. Hahn, and W. B. Mims, Phys. Rev. **137**, A61 (1965).
[18] J. Isoya, M. K. Bowman, J. R. Norris, and J. A. Weil, J. Chem. Phys. **78**, 1735 (1983).
[19] C. P. Poole, Jr., and H. A. Farach, *Theory of Magnetic Resonance* (John Wiley & Sons, New York, 1987), p. 57.
[20] J. R. Morton and K. F. Preston, J. Magn. Reson. (1969-1992) **30**, 377 (1978).
[21] R. Orbach and W. P. Wolf, Proc. R. Soc. London, Ser. A **264**, 458 (1961).
[22] Using average values for the effective mass of the donors and the static dielectric constants of 4*H*-SiC.
[23] W. R. L. Lambrecht and B. Segall, Phys. Rev. B **52**, R2249 (1995).
[24] E. Rauls, Th. Frauenheim, A. Gali, and P. Deák, Phys. Rev. B **68**, 155208 (2003).
[25] J. M. Soler, E. Artacho, J. D. Gale, A. Garciá, J. Junquera, P. Ordejón, and D. Sánchez-Portal, J. Phys.: Condens. Matter **14**, 2745 (2002).
[26] N. Troullier and J. L. Martins, Phys. Rev. B **43**, 1993 (1991).
[27] D. M. Ceperley and B. J. Alder, Phys. Rev. Lett. **45**, 566 (1980).
[28] J. P. Perdew and A. Zunger, Phys. Rev. B **23**, 5048 (1981).
[29] I. G. Ivanov, A. Henry, and E. Janzén, Phys. Rev. B **71**, 241201(R) (2005).
[30] I. G. Ivanov, B. Magnusson, and E. Janzén, Phys. Rev. B **67**, 165211 (2003).
[31] M. Bockstedte, A. Mattausch, and O. Pankratov, Appl. Phys. Lett. **85**, 58 (2004).
[32] E. Sörman, N. T. Son, W. M. Chen, O. Kordina, C. Hallin, and E. Janzén, Phys. Rev. B **61**, 2613 (2000).
[33] T. G. Castner Jr., Phys. Rev. Lett. **8**, 13 (1962).
[34] R. Püsche, M. Hundhausen, L. Ley, K. Semmelroth, G. Pensl, P. Desperrier, P. J. Wellmann, E. E. Haller, J. W. Ager, and U. Starke, *Proceedings of the International Conference on* SiC *and Related Materials 2005*, Pittsburgh, USA, September 18-23, 2005, Mater. Sci. Forum (to be published).
[35] D. J. Lépine, Phys. Rev. B **2**, 2429 (1970).
[36] C. Persson and U. Lindefelt, J. Appl. Phys. **82**, 5496 (1997).